Top-gate staggered poly(3,3‴-dialkyl-quarterthiophene) organic thin-film transistors with reverse-offset-printed silver source/drain electrodes

Minseok Kim[1,2], Jae Bon Koo[1,a], Kang-Jun Baeg[1], Soon-Won Jung[1], Byeong-Kwon Ju[2,a] and In-Kyu You[1]

+ VIEW AFFILIATIONS

a) Authors to whom correspondence should be addressed. Electronic addresses: kjb0706@etri.re.kr and bkju@korea.ac.kr.

📄 Download PDF

< PREVIOUS ARTICLE | TABLE OF CONTENTS | NEXT ARTICLE >

| Abstract | Full Text | References (24) | Cited By | Data & Media | Metrics | Related |

Here, we report on high-performance top-gated poly(3,3‴-dialkyl-quarterthiophene) (PQT-12) organic thin-film transistors (OTFTs) with reverse-offset-printed (ROP) silver (Ag) source/drain (S/D) electrodes. OTFT devices with ROP S/D electrodes using Ag nanopaste show higher performance (~ 0.01 cm^2/Vs) than those fabricated by vacuum electron beam evaporation with conventional photolithography and a standard lift-off process ($\sim 1 \times 10^{-3}$ cm^2/Vs). This dissimilarity is attributed to the higher work function (-4.9 eV) of the ROP Ag electrode due to AgO formation on the Ag surface during thermal annealing. This results in a low interfacial hole injection energy barrier between the S/D electrodes and the PQT-12 semiconductor.

Key Topics

Silver

Electrodes

Thin film transistors

Nanoparticles

Semiconductors

Gold

Semiconductor device fabrication

Organic semiconductors

Solvents

Work functions

Top-gate staggered poly(3,3-dialkyl-quarterthiophene) organic thin-film transistors with reverse-offset-printed silver source/drain electrodes

Minseok Kim, Jae Bon Koo, Kang-Jun Baeg, Soon-Won Jung, Byeong-Kwon Ju, and In-Kyu You

Top-gate staggered poly(3,3‴-dialkyl-quarterthiophene) organic thin-film transistors with reverse-offset-printed silver source/drain electrodes

Minseok Kim,[1,2] Jae Bon Koo,[1,a)] Kang-Jun Baeg,[1] Soon-Won Jung,[1] Byeong-Kwon Ju,[2,a)] and In-Kyu You[1]

[1]Convergence Components & Materials Research Laboratory, Electronics and Telecommunications Research Institute, Yuseong-gu, Daejeon 305-700, South Korea
[2]Display and Nanosystem Laboratory, College of Engineering, Korea University, Seongbuk-gu, Seoul 136-713, South Korea

Here, we report on high-performance top-gated poly(3,3‴-dialkyl-quarterthiophene) (PQT-12) organic thin-film transistors (OTFTs) with reverse-offset-printed (ROP) silver (Ag) source/drain (S/D) electrodes. OTFT devices with ROP S/D electrodes using Ag nanopaste show higher performance ($\sim$0.01 cm^2/Vs) than those fabricated by vacuum electron beam evaporation with conventional photolithography and a standard lift-off process ($\sim$1 $\times$ 10^{-3} cm^2/Vs). This dissimilarity is attributed to the higher work function (-4.9 eV) of the ROP Ag electrode due to AgO formation on the Ag surface during thermal annealing. This results in a low interfacial hole injection energy barrier between the S/D electrodes and the PQT-12 semiconductor. © 2012 American Institute of Physics. [http://dx.doi.org/10.1063/1.4755878]

Organic opto/electronic devices can be used in a wide range of applications, such as flat panel or flexible displays,[1] photovoltaics,[2] flash memory,[3] radio frequency identification tags,[4] and bio-/chemical-sensors.[5] Furthermore, the use of solution-processable π-conjugated organic materials as active elements in those applications offers great potential for large-area, flexible, and ultra low-cost electronics.[6] Over the last several years, research has been increasingly concentrated on the development of functional inks—from functional organic materials to solution-processed metal electrodes—and their processing methods for printed electronic devices. These printing methods have been attracting great attention due to their simple and cheap processes compared with the conventional photolithography process, which requires many subunitary processes–including coating or deposition, cleaning, masking, etching, and stripping—to achieve a single patterned layer. To this end, a variety of both micro- and macro-electronics printing techniques have been reported including spray printing,[7] nano-imprinting,[8] screen printing,[9] inkjet printing,[10] flexography,[11] gravure,[12] and offset printing,[13] which are mostly only intended for individual components of conductors, semiconductors, and insulators, but may also be used for fully printed devices.

Although graphic art printing methods have been demonstrated, resulting in proper electronic device performance, those processes were mainly applied partially, either for electrodes, active layers, or dielectrics, in the fabrication of the devices. Therefore, for application of these printing processes to extremely low-cost organic electronics with mechanical flexibility and large area, it is imperative to use continuous web-based roll-to-roll (R2R) machinery. However, the results reported to date have typically shown that mass R2R printed devices had poor device performance compared with similar devices prepared using spin coating,

inkjet printing, or photolithographic patterning. Recently, Moon et al.[14] analyzed a direct printing method using Ag nanopowder ink for metal electrodes; this was a modified version of conventional gravure offset printing. They first coated a soft blanket roll with Ag ink and rolled it onto a glass cliché with electrode patterns. This pickup (off-step) process removes any unnecessary Ag ink outside the intaglio patterns. They then transferred the remaining Ag ink on the blanket roll to the desired glass substrate (set-step). This method is commonly called reverse offset printing (ROP) and is one of the mass-production printing methods that can achieve high resolution and complicated shape patterns.

In this study, we investigated top-gate poly(3,3‴-dialkyl-quarterthiophene) (PQT-12) thin-film transistors (TFTs) with staggered source/drain (S/D) electrodes, which were fabricated by ROP with Ag nanoparticle paste. The organic thin-film transistor (OTFT) properties were compared to those of devices made by vacuum electron beam evaporation (VEBE) with conventional photolithography and lift-off processes. These transistors showed dissimilar electrical properties, which originated from the interfacial energy barrier difference between PQT-12 and Ag electrodes fabricated by different methods.

Ag electrodes were printed on glass substrates by using a roll plate-to-plate ROP (Narae Nanotech Co.). Ag paste ink, which is made of nanoparticles (Ag content: 39 wt. %, viscosity: 1.5 cPs at 0.4 rpm, surface tension: 25.8 mN/m; Advanced Nano Products Co., Ltd.), was dispensed onto the surface of the poly-dimethylsiloxane blanket roll (KNW Co.). A small amount of Ag nanopaste ink can be manipulated by a syringe pump. Glass cliché was prepared through the wet-etching process using a Cr metal mask and hydrogen fluoride. As the blanket was rolled over the cliché with intaglio patterns, unnecessary ink was removed from the blanket and transferred onto the top of the cliché surface. The remaining Ag ink, which was in the desired pattern on the blanket, was transferred onto 100 × 100 mm glass substrates

---

a)Authors to whom correspondence should be addressed. Electronic addresses: kjb0706@etri.re.kr and bkju@korea.ac.kr.
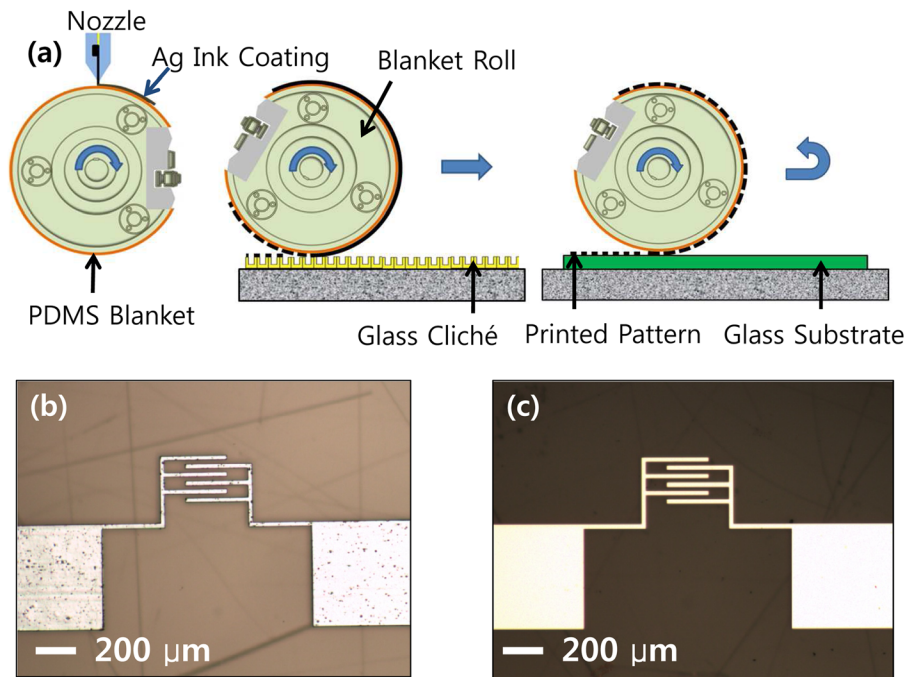
101, 133306-1

FIG. 1. (a) Schematic diagrams of reverse offset printing process. Optical images of the source/drain silver electrodes fabricated (b) by reverse offset printing and (c) by vacuum electron beam evaporation. (*W/L*: 1000 μm/20 μm) (thickness: 400–450 μm).

(Corning, Eagle XG) (Fig. 1(a)). In order to remove the various additives and residual solvent in the printed Ag ink, the heat treatment for sintering was performed at 350 °C on a hotplate for 20 min in air. The nanoparticles and the printed surface morphology of the Ag ink were observed using a high-resolution transmission electron microscope (HR-TEM) (JEOL, JEM 3010) and a scanning electron microscope (SEM) (Sirion 400). The specific resistance of printed Ag electrodes was calculated from the sheet resistance and the thickness found by using a four-point probe and a surface profiler (Tencor, Alpha-Step IQ), respectively. The contact potential difference of the printed Ag electrode was detected by a Kelvin probe (KP 6500 Digital Kelvin probe, McAllister Technical Services, Co., Ltd.).

Regioregular PQT-12 (American Dye Source, MW = 25 k) was dissolved in 1,2-dichlorobenzene (20 mg/ml) on a hotplate at 80 °C for 30 min before being filtered via a 0.2 μm polytetrafluoroethylene syringe filter; it was then spin-coated at 2000 rpm onto the Ag electrodes patterned substrate as an active semiconductor layer. After thermal annealing at 135 °C for 20 min in a N_2-filled glove box, poly(methyl methacrylate) (PMMA) (Sigma Aldrich, MW = 120 k, dielectric constant ε_r = 3.5) was dissolved in *n*-butyl acetate (nBA) (120 mg/ml) at 80 °C for more than 5 h and spin-coated at 2000 rpm to form a gate dielectric layer (thickness, $t \sim 1.2\ \mu$m). The film was then baked at 100 °C for 30 min to remove the solvents in the N_2-filled glove box. Finally, for the gate electrode, an Al film ($t \sim 100$ nm) was deposited by thermal evaporation through a metal shadow mask. Control devices based on conventional VEBE and a lift-off process were prepared for comparison. The S/D electrodes of ROP-based Ag and VEBE-based Ag were prepared with the same shape and thickness ($t \sim 450$ nm) (Figs. 1(b) and 1(c)). After device fabrication, the electrical characteristics of the PQT-12 TFTs were measured using a KEITHLEY 4200-SCS semiconductor parameter analyzer under dark and ambient air conditions. The field-effect mobility (μ_{FE}) and

threshold voltage (V_T) of the transistors were calculated in the saturation region using the gradual channel approximation.[15]

The thermal behavior of Ag ink was examined by a thermogravimetric analysis and a differential scanning calorimeter (TGA/DSC) (Setsys 16/18) with a 10 °C/min scanning rate in N_2. As shown in Figs. 2(a) and 2(b), the weight loss of Ag ink was continuously observed over the temperature ranging from 25 to 500 °C; the weight loss profile was found to have three distinct temperature regions. The first significant weight loss of Ag ink was observed at around 100 °C and is due to moisture desorption from the Ag nanopaste. The second significant weight loss at around 172 °C is attributed to the decomposition of the organic molecular residues such as surfactant, solvent, and additives added during the synthesis of Ag nanopaste.[16] As shown in Fig. 2(b), the third exothermic peak was observed at 220 °C and can be attributed to the crystallization of Ag nanoparticles or recrystallization of strained Ag nanoparticles.[17] Hence, it is considered that significant grain growth of the Ag nanopaste occurred at around 220 °C (Figs. 2(c)–2(e)).

The particles of the prepared Ag nanopaste were almost monodispersed, and the sizes of the particles were in the range of 3 to 10 nm, as measured by HR-TEM (Fig. 2(f)). The particles were easily dispersible with common organic solvents such as octane and toluene. This would enable easy self-assembly of these particles into a close-packed array when printed, thus considerably facilitating their conglutination into continuous conductive lines.[18] The surface microstructure of the Ag electrode was observed with a SEM. With increasing curing temperature, the grain growth and the densification of the Ag nanoparticles were increased, resulting in high electrical conductivity. At the curing temperature of 150 °C, the calculated specific electrical resistance of the Ag nanopaste was a few kΩ cm, which is not suitable for an electrical conductor. At 250 °C, however, it was decreased to 5.4×10^{-6} Ω cm because of significant densification with grain size growth and crystallization of the Ag nanoparticles
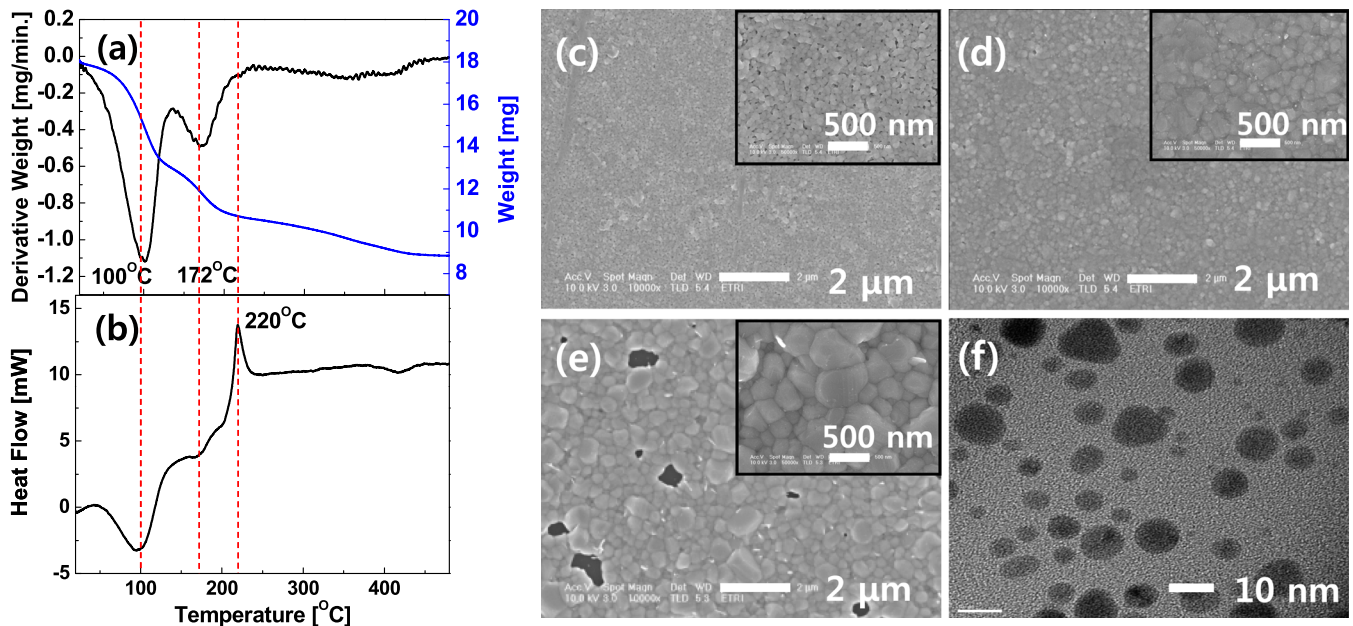
FIG. 2. (a) TGA and (b) DSC of the silver nanopaste ink. SEM images of silver nanopaste cured at (c) 250, (d) 350, and (e) 450 °C. Inset images are magnification. (f) HR-TEM image of silver nanoparticles.

(Fig. 2(c)). At 350 °C, the minimized specific resistance of 2.8×10^{-6} Ω cm and the densest electrical conduction electrode without disconnected regions were obtained as shown in Fig. 2(d). This is high enough to serve in an integrated circuit as electrical conduction lines. At 450 °C, discontinuous and disconnected regions on the surface microstructure were observed as shown in Fig. 2(e). This was attributed to Ag compounds that coalesced at excessively high thermal annealing temperatures. This leads to increased resistance caused by the disrupting of the surfaces of conduction lines.[19]

ROP Ag electrodes were applied to the source/drain (S/D) electrodes of the top-gate/bottom-contact (TG/BC) staggered OTFTs based on p-type polymer semiconductor (PQT-12) [see Fig. 3(a)]. A control device with VEBE-based Ag S/D electrodes was fabricated by a conventional lift-off process and with identical geometry and thickness as that of the ROP Ag. PMMA polymer gate dielectric was spin-coated onto the semiconductor layer using orthogonal solvent (nBA) to under-lay the films. The transfer and output characteristics of PQT-12 TFTs with VEBE-based Ag electrodes are shown in Figs. 3(b) and 3(c), and those with ROP-based Ag electrodes can be seen in Figs. 3(d) and 3(e). The extracted fundamental OTFT parameters of those devices are summarized in Table I. The μ_{FE} in the saturation region ($V_G - V_T < V_D$) is calculated from the following equation:

$$\left. \frac{\partial \sqrt{I_D}}{\partial V_G} \right|_{V_D} = \sqrt{\frac{W}{2L} C_i \mu(sat)}, \qquad (1)$$

where I_D is the source-to-drain current; W and L are the channel width and length, respectively; C_i is the dielectric capacitance per unit area; V_G is the gate voltage; V_T is the threshold voltage; and V_D is the source-to-drain voltage. The V_T value was calculated from the x-axis intercept of the line obtained by plotting the square root of I_D versus V_G. The subthreshold swing (S) that measures how rapidly the device switches from the off state to the on state in the region of
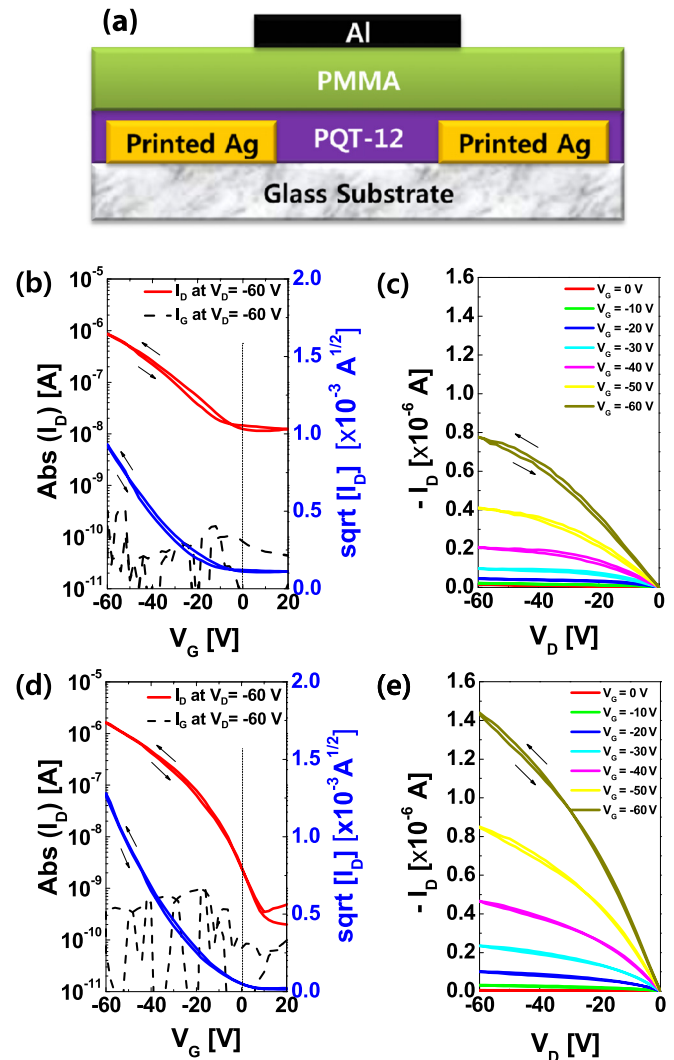

FIG. 3. (a) Schematic diagram of a top-gate staggered transistor with the S/D electrodes printed by reverse offset printing. Electrical characteristics of PQT-12 OTFTs with VEBE-based Ag electrode ((b) and (c)), and ROP-based Ag electrode ((d) and (e)). PMMA dielectric ($t \sim 1.2\ \mu m$, $C_i \sim 2.6$ nF/cm^2), ($W/L = 1000\ \mu m /20\ \mu m$).

TABLE I. Transistor parameters[a] for top-gate staggered OTFT.

Active	S/D Ag electrodes (thickness)	μ_{FE}[b] (cm^2/Vs)	V_T (V)	I_{on}/I_{off}	S (V/decade)
PQT-12 (2 wt. %)	VEBE-based (450 nm)	0.007	−17.4	~10^2	−35
	ROP-based (450 nm)	0.016	−20.6	~10^4	−8

[a]Field-effect mobility (μ_{FE}), current on-off ratio (I_{on}/I_{off}), threshold voltage (V_T), and subthreshold swing (S).
[b]The field-effect mobility values were calculated in the saturation region ($V_D = -60$ V).

exponential current increase was calculated from the following equation:[15]

$$S = \frac{dV_G}{d(\log I_D)}.$$ (2)

The OTFTs based on the VEBE Ag S/D electrodes exhibited poor device performance with a μ_{FE} value of 0.007 cm^2/Vs, an on/off current ratio (I_{on}/I_{off}) of 1×10^2, a V_T of −17.4 V at $V_D = -60$ V, and an S of −35 V/decade without significant bias hysteresis. In contrast, the OTFTs with ROP-based Ag S/D electrodes showed relatively high performance with a μ_{FE} of 0.016 cm^2/Vs, an I_{on}/I_{off} of 1×10^4, a V_T of −20.6 V at $V_D = -60$ V, and a S of −8 V/decade without hysteresis. In addition, we fabricated a PQT-12 TFT with VEBE-based Au/Cr electrodes (Au/Cr, 20/3 nm thick) as a reference device. The μ_{FE} of this device was on the order of 0.1 cm^2/Vs which was one order higher than that with the ROP-based Ag electrode, with an I_{on}/I_{off} of 1×10^3, V_T of −10.5 V at $V_D = -60$ V, and S of −13 V/decade. Although the device performance of the PQT-12 TFT with ROP-based Ag electrodes has not yet reached that of the VEBE-based Au/Cr electrodes, it may still be a good candidate for low-cost printed electronics. The device properties can be further improved through special surface treatments including the use of self-assembly monolayers (SAMs) and carrier injection layers. Note that the leakage current (I_G) of all devices was less than a few nm.

The observed difference in the transfer characteristics of the PQT-12 TFTs depending on the different processing of the electrodes is attributed to an aspect of the charge carrier injection between the semiconductor frontier molecular orbital and the metal electrode. We measured the work function of the ROP-based Ag and the VEBE-based Ag electrodes by Kelvin probe force measurement, and they were found to be −4.96 and −4.71 eV, respectively. With increasing the curing temperature, it can be seen that the work function of the ROP-based Ag is mostly decreased except for 450 °C, though that of the VEBE-based Ag is practically identical. Note that the ROP-based Ag cured at 350 °C was used for S/D electrodes in this paper. PQT-12 was known for having the highest occupied molecular orbital (HOMO) level of −5.24 eV.[20] The interfacial energy barrier between the PQT-12 and the ROP-based Ag was ~0.28 eV, and that of the VEBE-based Ag was ~0.53 eV. This indicates that the hole injection barrier from the ROP-based Ag S/D to the HOMO level of PQT-12 is lower than that of VEBE-based Ag S/D.[21] This explains the origin of the observed relatively high OTFT performance with the ROP-based Ag electrodes. The x-ray photoelectron spectroscopy

(XPS) results reveal that the work function of the ROP-based Ag increased due to the formation of silver oxide (AgO). As can be seen in Fig. 4(b), the peaks at 532 eV represent the core level of an oxygen atom (that is, the 1 s orbital), which exhibited significantly large intensity in the ROP-based Ag in contrast to the case of the VEBE-based Ag. The formation of AgO presumably resulted from the curing process at relatively high temperatures as well as the Ag nanopaste ink itself because some of the additives could become diverse oxygen sources. AgO has been reported to show *p*-type semiconducting properties with Fermi levels of from −4.8 to −5.1 eV and has also been used as a hole-transport layer in organic light-emitting diodes[22] and polymer solar cells;[23] those approaches are consistent with the results obtained in this work. Although the OTFT device performance needs to be optimized, we expect that our high resolution and high throughput roll plate-to-plate ROP Ag electrodes can be utilized in a variety of extremely low-cost printed electronics applications and integrated circuits with high performance.

High performance top-gate PQT-12 OTFTs with staggered Ag S/D electrodes were demonstrated by using the roll plate-to-plate ROP method. The electrical characteristics of
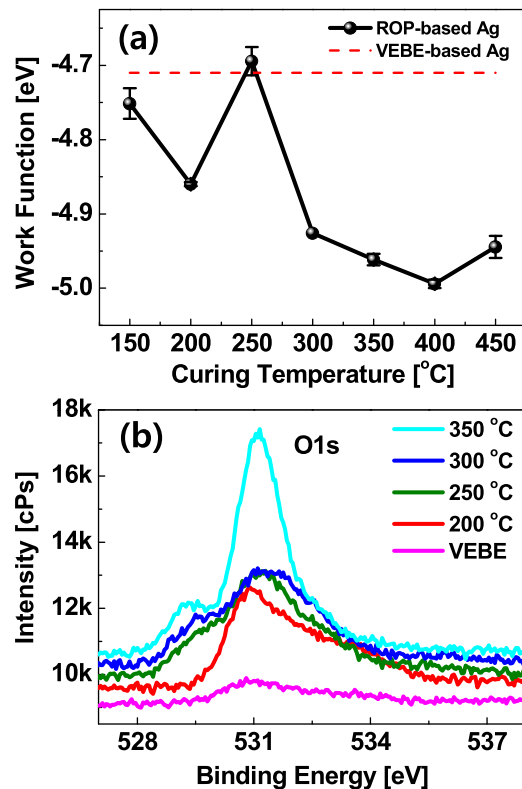

FIG. 4. (a) Work function of the ROP Ag and the VEBE Ag electrodes, (b) XPS spectra of oxygen atom.

those OTFT devices were shown to have a relatively high μ_{FE} ($\sim$0.01 cm^2/Vs), more than one order of magnitude than that of control devices with VEBE-processed Ag S/D ($\sim$0.001 cm^2/Vs). This was mainly attributed to the lower energetic barrier for efficient charge injection from the Ag metal electrode to the PQT-12 organic semiconductor. XPS and Kelvin probe force measurements revealed that the formation of the AgO during the thermal annealing process clearly leads to a higher work function for ROP-Ag S/D electrodes. After optimization of the device performance, as well as integration with complicated electronic circuits, we expect that the high resolution and high throughput roll-to-roll printable Ag metal electrodes will be utilized in a variety of low-cost printed electronics applications.

[1]G. H. Gelinck, H. E. A. Huitema, E. V. Veenendaal, E. Cantatore, L. Schrijnemakers, J. B. P. H. V. D. Putten, T. C. T. Geuns, M. Beenhakkers, J. B. Giesbers, B.-H. Huisman, E. J. Meijer, E. M. Benito, F. J. Touwslager, A. W. Marsman, B. J. E. V. Rens, and D. M. D. Leeuw, Nature Mater. **3**, 106 (2004).
[2]S. R. Forrest, Nature **428**, 911 (2004).
[3]K.-J. Baeg, D. Khim, J. Kim, B.-D. Yang, M. Kang, S. W. Jung, I.-K. You, D.-Y. Kim, and Y.-Y. Noh, Adv. Funct. Mater. **22**, 2915 (2012).
[4]R. Rotzoll1, S. Mohapatra, V. Olariu, R. Wenz, M. Grigas, K. Dimmler, O. Shchekin, and A. Dodabalapur, Appl. Phys. Lett. **88**, 123502 (2006).
[5]B. Crone, A. Dodabalapur, A. Gelperin, L. Torsi, H. E. Katz, A. J. Lovinger, and Z. Bao, Appl. Phys. Lett. **78**, 2229 (2001).
[6]S. Allard, M. Forster, B. Souharce, H. Thiem, and U. Scherf, Angew. Chem., Int. Ed. **47**, 4070 (2008).
[7]K.-J. Baeg, J. Kim, D. Khim, M. Caironi, D.-Y. Kim, I.-K. You, J. R. Quinn, A. Facchetti, and Y.-Y. Noh, ACS Appl. Mater. Interfaces **3**, 3205 (2011).
[8]S. H. Ahn and L. J. Guo, ACS Nano **3**, 2304 (2009).
[9]D. A. Pardo, G. E. Jabbour, and N. Peyghambarian, Adv. Mater. **12**, 1249 (2000).
[10]Y.-Y. Noh, N. Zhao, M. Caironi, and H. Sirringhaus, Nature Nanotechnol. **2**, 784 (2007).
[11]T. Mäkelä, S. Jussila, H. Kosonen, T. G. Bäcklund, H. G. O. Sandberg, and H. Stubb, Synth. Met. **153**, 285 (2005).
[12]H. Yan, Z. Chen, Y. Zheng, C. Newman, J. R. Quinn, F. Dötz, M. Kastler, and A. Facchetti, Nature **457**, 679 (2009).
[13]D. Zielke, A. C. Hübler, U. Hahn, N. Brandt, M. Bartzsch, U. Fügmann, T. Fischer, J. Veres, and S. Ogier, Appl. Phys. Lett. **87**, 123508 (2005).
[14]T.-H. Moon, S.-H. Nam, N.-K. Kim, Y.-K. Kook, Y.-K. Jung, Y.-G. Chang, S.-S.Yoo, C.-D. Kim, I. Kang, and I.-J. Chung, SID Int. Symp. Digest Tech. Papers **40**, 1348 (2009).
[15]S. M. Sze and K. K. Ng, *Physics of Semiconductor Devices*, 3rd ed. (Wiley-Interscience, New York, 2007).
[16]R. Zhang, K.-S. Moon, W. Lin, and C. P. Wong, J. Mater. Chem. **20**, 2018 (2010).
[17]D. Kim and J. Moon, Electrochem. Solid-State Lett. **8**, J30 (2005).
[18]Y. Wu, Y. Li, and B. S. Ong, J. Am. Chem. Soc. **128**, 4202 (2006).
[19]J.-W. Park and S.-G. Baek, Scr. Mater. **55**, 1139 (2006).
[20]B. S. Ong, Y. Wu, P. Liu, and S. Gardner, Adv. Mater. **17**, 1141 (2005).
[21]C. Yun, M. Kim, S. W. Lee, H. Moon, S. Park, J. B. Koo, J. W. Kim, I.-K. You, and S. Yoo, IEEE Electron Device Lett. **32**, 1454 (2011).
[22]C.-W. Chen. P.-Y. Hsieh, H.-H. Chiang, C.-L. Lin, H.-M. Wu, and C.-C. Wu, Appl. Phys. Lett. **83**, 5127 (2003).
[23]J. B. Kim, C. S. Kim, Y. S. Kim, and Y.-L. Loo, Appl. Phys. Lett. **95**, 183301 (2009).